Structural, Chemical and Optical Properties of Cerium Dioxide Film Prepared by Atomic Layer Deposition on TiN and Si Substrates

S. Vangelista[1], R. Piagge[2], S. Ek[3], T. Sarnet[3], G. Ghidini[2], C. Martella[1] and A. Lamperti[1]

[1]CNR-IMM - MDM Laboratory, Via C. Olivetti 2, Agrate Brianza (MB) I-20864 Italy

[2]STMicroelectronics, Via C. Olivetti 2, Agrate Brianza (MB) I-20864 Italy

[3]Picosun Oy, Tietotie 3, Espoo FI-02150 Finland

This work is licensed under the Creative Commons Attribution-Non Commercial-No Derivs 2.5 Italy License. To view a copy of this license, visit http://creativecommons.org/licenses/by-nc-nd/2.5/it/ or send a letter to Creative Commons, PO Box 1866, Mountain View, CA 94042, USA.

Thin films of cerium dioxide (CeO_2) were deposited by atomic layer deposition (ALD) at 250 °C on both Si and TiN substrates. The ALD growth produces CeO_2 films with polycrystalline cubic phase on both substrates. However, the films show a preferential orientation along <200> crystallographic direction for CeO_2/Si or <111> for CeO_2/TiN, as revealed by X-ray diffraction. Additionally, CeO_2 films differ in interface roughness depending on the substrate. Furthermore, the relative concentration of Ce^{3+} is 22.0% in CeO_2/Si and around 18% in CeO_2/TiN, as obtained by X-ray photoelectron spectroscopy (XPS). Such values indicate a ~10% off-stoichiometry and are indicative of the presence of oxygen vacancies in the films. Nonetheless, CeO_2 bandgap energy and refractive index at 550 nm are 3.54±0.63 eV and 2.3 for CeO_2/Si, and 3.63±0.18 eV and 2.4 for CeO_2/TiN, respectively. Our results extend the knowledge on the structural and chemical properties of ALD-deposited CeO_2 either on Si or TiN substrates, underlying films differences and similarities, thus contributing to boost the use of CeO_2 through ALD deposition as foreseen in a wide number of applications.

1. INTRODUCTION

In the last years, CeO_2 based materials have attracted much attention due to their wide use in many application areas such as catalysis, hydrogen production, gas sensing and electrodes in fuel cells [1,2 ,3 ,4 ,5]. In microelectronics, CeO_2 has been considered as high κ-gate oxide material due to its unique properties: moderate band gap (3–3.6 eV), high dielectric constant (κ: 23–26), high refractive index (n: 2.2–2.8) and high dielectric strength (~2.6 MV cm^{-1}) [6]. CeO_2 is also suitable for Si based metal oxide semiconductor (MOS) devices due to its small lattice mismatch (−0.35%) with Si that favors its epitaxial growth on different silicon surfaces [7] and low interface-state density (~ 10^{11} $cm^{-2}eV^{-1}$) [5,8]. CeO_2 use was explored also for non-volatile memory devices in metal-insulator-metal stacks [9]. For catalytic applications CeO_2 has to be grown on metallic substrates; however, few studies exist on cerium oxide film grown on metals and with ultra-low thickness (mono or few layers) aiming at depicting the epitaxial growth relation [10and references therein].

CeO_2 deposition is achieved by using a variety of growth techniques, such as e-beam [11], physical vapor deposition [12], RF-magnetron sputtering [13], chemical vapor deposition (CVD) [14,15 ,16 ,17 ,18], even in sub-stoichiometric form (CeO_{2-x}, $0<x<0.4$) [19]. However, when highly stoichiometric oxide is required, atomic layer deposition (ALD) is the most suitable technique. ALD is a self-limiting technique, based on sequential surface reactions. Moreover, ALD allows the atomic layer control of the film thickness with large-area uniformity and conformality also on 3D surfaces. Further, thin films deposition can be performed at lower temperatures than other vacuum deposition techniques such as pulsed laser deposition or CVD, a process condition that guarantees low thermal budget, no or limited interdiffusion phenomena, and the possibility to use temperature-sensitive substrates. ALD deposition of CeO_2 on Si or Si/SiO_2 substrates has been

explored by using various precursors [20,21 ,22 ,23 ,24 ,25 ,26 ,27], obtaining as-deposited film with polycrystalline structure [22-25] which influences the dielectric behavior [24]. However, ALD of CeO_2 on metal substrates (or electrically behaving as metals, such as TiN) has not been explored yet.

In this work, we aim to a deep understanding of the structural properties of ALD-deposited CeO_2 either on Si or TiN substrate, underlying the differences and similarities in the properties of the obtained films. Our results will contribute to give the basis for the use of CeO_2 through ALD deposition as foreseen in a wide number of applications, in particular in microelectronics and catalysis.

2. Experimental section

Cerium dioxide thin films were deposited in a Picosun R-200 Advanced ALD reactor by Picosun Oy. The precursor $Ce(thd)_4$ (thd = 2,2,6,6-tetramethyl-3,5-heptanedione) was evaporated at the temperature of 140 °C and ozone has been used as oxidizing agent (concentration 19%). Both precursors were transported into the reactor chamber by N_2 carrier gas flow. Based on the results reported in ref. [22], the deposition temperature was chosen as 250 °C, the pulse times for $Ce(thd)_4$ and ozone were 1.0 s and 2.5 s respectively, and the purge time with nitrogen after pulses was 1.5 s. Under these conditions the growth rate was 0.32 Å/cycle. The targeted oxide thickness on both substrates was 25 nm. The deposition was done on both Si and TiN-coated 7x7 cm^2 Si substrates simultaneously, by placing them on an 8" silicon wafer which was put in the wafer holder. TiN coating layers, nominally 7 nm thick, have been deposited by CVD.

X-ray reflectivity (XRR) and diffraction at grazing incidence (GIXRD) have been performed using an XRD3000 diffractometer (Italstructure) with monochromated X-ray Cu Kα radiation

(wavelength 0.154 nm) and beam size defined by slits aperture of 0.1 × 6 mm. Data fitting, performed using MAUD program [28], allowed us to determine thickness, interface and surface roughness, and electronic density. MAUD has also been used for Rietveld refinement of GIXRD patterns, allowing to determine CeO_2 cell parameter and grain size [29].

The morphology of the samples was investigated in tapping mode by means of an AFM-Bruker commercial system, equipped with ultrasharp silicon probes (nominal tip radius ~10 nm). Root-mean-square (rms) roughness and other statistical parameters of the surface morphology were quantitatively derived from the topographies employing the free-available WSxM software.

Focus-ion-beam scanning electron microscopy (SEM) has been used to prepare cross sections of selected samples. Energy Dispersive X-ray Analysis (EDX, Oxford X-MAS 80 mm^2) in STEM mode was acquired in a Transmission Electron Microscope (TEM, Fei Tecnai G2) operating at 200 kV. EDX allows for the identification of the chemical composition with a detection limit ~ 1% for the analysed elements.

The compositional depth profile of the CeO_2/TiN/Si and CeO_2/Si structures was also investigated by Time of Flight-Secondary Ion Mass Spectrometry (ToF-SIMS) by means of a Cs^+ ion beam (energy of 0.5 keV, ion current 38.5 nA) sputtering a 200 μm × 200 μm area, and Ga^+ ion beam (25 keV, 2.7 pA) for analysis over a 50 μm × 50 μm area centred on the sputtered crater and therein collecting secondary negative ions [30].

To gain a deep knowledge on the chemical state of the CeO_2 [31] films, X-ray photoelectron spectroscopy (XPS) measurements were performed on a PHI 5600 instrument (Physics Electronics Inc.) equipped with a monochromatic AlKα X-ray source (energy = 1486.6 eV) and a concentric hemispherical analyser. The spectra were collected at a take-off angle of 45° and band-pass energy of 23.50 eV. The instrument resolution is 0.5 eV. The spectra were aligned using *C 1s* peak (284.6

eV) as reference [32]. The experimental data were fitted with Gaussian-Lorentzian peaks and Shirley background by using XPSPeak program (version 4.1, Freeware, University of Warwick, United Kingdom). The spin-orbit splitting and doublet intensity ratio values have been fixed from literature [33].

Spectroscopic Ellipsometry (SE, Woollam M-2000 F) was used to acquire spectra in the visible-UV range from 1.24 to 5.05 eV. The ellipsometric angle ψ and phase difference Δ were recorded at an incidence angle of 75°. The optical dielectric function of CeO_2 was obtained by using a model of two Tauc–Lorentz (2TL) oscillators by using EASE program (J.A. Woollam Co., Inc.), allowing to obtain the refractive index and the direct and indirect band gaps.

3. Results and Discussion

XRR of as-deposited films on Si and TiN substrates are shown in **figure 1(a)** and in **figure 1(b)**, **respectively**. The values of thickness, roughness and electronic density obtained from the fitting are reported in **Table 1**. CeO_2 thickness is close to the target (25 nm) in both cases, as confirmed also by TEM (not shown). The interface roughness is higher in the CeO_2/TiN sample than in the CeO_2/Si sample; in addition, a very thin oxidation of TiN surface is detected. The calculated electronic density of CeO_2 films is slightly below the bulk value (1.79 $e^-/Å^3$), nonetheless in line with the considerations that we are measuring thin films at the nanoscale with the presence of contaminants (mainly C and OH) from $Ce(thd)_4$ precursor decomposition [22]. The surface roughness is limited to 1.4 nm. On the top of the as-deposited films the absorption of humidity is detected, a well-known phenomenon for CeO_2 [34], due to its intrinsic hygroscopicity. The presence of humidity at the surface has been detected also by performing AFM measurements of the samples, in particular for CeO_2/TiN. Despite the strong water-tip interaction, we managed to

acquire the surface images of the samples (see the inset of the figure 1(a) and 1(b)) and to calculate grain size and RMS roughness: in both samples, we found around 15 nm and 1.2 nm, respectively. Thus, AFM analysis confirms XRR findings.

The crystallinity of the films was examined by GIXRD at fixed incidence angle of 2°. **Figure 2** shows the GIXRD patterns of as-deposited CeO_2 film on Si and TiN substrates. Both films are polycrystalline, exhibiting the typical peaks of a face centered cubic (fcc) structure (*Fm-3m* in space group notation), as reported in the crystallographic database [35]. No signal coming from the TiN layer is detected (TiN layer is 7.2 nm thick from XRR), indicating its amorphous nature – as confirmed by TEM (not shown).

More in detail, the observed relative intensity of CeO_2 peaks gives an indication of some preferential orientation. This evidence becomes clear by performing Rietveld refinement of the GIXRD data assuming the powder pattern as initial input (see the continuous lines on top of the experimental dot points in **figure 2**). For CeO_2 deposited on TiN (lower black dots with red line) the I_{111}/I_{200} intensity ratio is higher than that of the powder spectrum, while for the CeO_2 deposited on Si (upper blue dots with light blue line) the I_{111}/I_{200} intensity ratio is lower than that of the powder diffraction pattern, the latter observation in accordance with ref. [36].

These findings suggest that CeO_2 growth is influenced by the different nature of the surface/layer onto which it is deposited. It is likely that the presence of a higher roughness at the CeO_2/TiN interface with respect to the case of CeO_2/SiO_2 could contribute in changing the energy requirement for the nucleation of crystals with *(111)* orientation. Atomistic simulations [37,38] show that the formation of crystallites exposing *(100)* surfaces is unstable because of the dipole generated perpendicular to it. However, the formation of polycrystalline CeO_2 with all crystalline orientations is well-demonstrated experimentally by using different growth methods [22], [25],

[39] and more generally it can be justified considering defects or charge compensating species, i.e. oxygen vacancies due to Ce^{3+}: Ce^{4+} substitution. In our case, the contaminants (C and OH) from the precursor can act as source of defects, or oxygen vacancies could be present due to a different reactivity of TiN versus Si. Further, using Sherrer's formula applied to the *(111)* and *(200)* peaks to estimate the size of the crystallites, the grains with *(200)* orientation result to be slightly larger than the *(111)*-oriented grains for CeO_2 films grown on both TiN and Si substrates, as reported on **Table 1**. However, before any other consideration, we remind the isotropic approximation in the Sherrer's implies that the crystalline grains are considered spherical, i.e. with the same dimension in all the crystallographic directions. This is likely not to be realistic in thin films, and the grains belonging to different orientations assume different shape and/or different distribution through the layer thickness.

In order to understand the presence and the nature of the contaminants in CeO_2 films we performed EDX and ToF-SIMS analysis. In **figures 3(a)** and **3(b)** we report ToF-SIMS chemical depth profiles for CeO_2 deposited on Si and on TiN respectively, together with the corresponding chemical maps of the elements in the layers from EDX (upper panels). At first, we observe that the CeO_2/Si interface is very sharp (**figure 3(a)**), with the existence of a thin silicon native oxide layer. On the other side, the CeO_2/TiN interface is slight broad (**figure 3(b)**), with the signals related with TiN showing not negligible tails in the oxide film region. This is possibly due to the roughness of the CeO_2/TiN interface rather than an onset of Ti diffusion into the CeO_2 film, also considering the low growth temperature (250 °C). Moreover, ToF-SIMS allows following the signals coming from C and OH, which are the typical spurious elements incorporated during an ALD deposition when heptanedionate (thd) and ozone precursors are used [22]. By comparing the levels of the signals, we observe that C intensity is comparatively lower in CeO_2/TiN than in

CeO_2/Si, while OH shows almost the same intensity. However, also in the worst case (i.e. CeO_2/Si) the correspondent C amount is only few atomic percent, as expected [22]. In any case, it is important to underline the presence of carbon, eventually in presence also of shortage of oxygen, since it can induce the reduction of Ce^{4+} into Ce^{3+}, which is fundamental in the use of ceria as catalytic converter [40].

The presence of Ce^{3+} can be related to defects in CeO_2, such as oxygen vacancies related with the oxygen storage capacity of CeO_2 [41], i.e. to a highly non-stoichiometric CeO_{2-x} phase [42]. A Ce_2O_3-like phase cannot be in principle excluded, but we do not have indication of Ce_2O_3 phase in the diffraction profiles, even in films annealed at high temperature.

The off-stoichiometry of the oxide can be estimated from the XPS analysis. Despite the technique probing volume is limited to the outermost part of the CeO_2 layers, which can convey of the interaction with the atmosphere, from the Ce^{3+}/ Ce^{4+} ratio estimation we can have indication of the chemical stoichiometry of the whole oxide layer. **Figures 4(a)** and **4(b)** show the *Ce 3d* and *O 1s* spectra of CeO_2 on Si (upper panel) and on TiN (lower panel). The figures show also the fit obtained from the deconvolution of the spectra into the different components, similarly to that reported in refs. [18, 42, 43, 44]. The analysis of the *Ce 3d* spectrum is particularly complex since the deconvolution considers 5 different doublets related to the two oxidation states due to primary photoionization and shake-down satellites: three related to the Ce^{4+} doublets and the other two related to the Ce^{3+} doublets. These components are reported in **Table 2** and labelled by following the rule that *u* and *v* refer to the $3d_{3/2}$ and $3d_{5/2}$ spin–orbit components, respectively. In **Table 2** the binding energies and relative peak areas are also reported.

By comparing the *Ce 3d* (and *O 1s*) spectra of the two cases the presence of a shift of one signal respect to the other is immediately evident and reveals the different chemical environment in the

two samples, since the spectra have been aligned to *C 1s* peak at 284.6 eV. From the area of the different components of the *Ce 3d* spectrum (**Table 2**) we estimate the Ce^{3+} and Ce^{4+} relative concentration [36], resulting in a Ce^{3+} concentration of 21.8% in CeO_2/Si, and 18.0% in CeO_2/TiN. Similarly, considering O 1s region, 2 components are identified and, from low to high binding energy (B.E.), assigned to oxygen bonded to Ce and adsorbed – OH/CO_3^{2-} complexes from the environment [18,45]. Since it is well-known that Ce^{3+} oxidation state is preferentially located at the surface of the oxide film [42] which is attributed to the interaction with organics in the air, we can assume that the Ce^{3+} percentage represents the upper limit of the off-stoichiometry for CeO_2 layers in both cases. Considering that the O/Ce ratio stoichiometry in a fully oxidized film is 2 for CeO_2 or 3/2 for Ce_2O_3 and considering the calculated concentrations for Ce^{3+} and Ce^{4+}, we obtain an O/Ce ratio of 1.89 for CeO_2/Si and 1.91 for CeO_2/TiN. Such values indicate a ~10% off-stoichiometry and suggest that Ce^{3+} is possibly related with the presence of oxygen vacancies in CeO_2 film, rather than Ce_2O_3 amorphous phase. Nonetheless, the difference of Ce^{3+} amount between CeO_2/Si and CeO_2/TiN, despite small, could be sufficient for inducing a different preferential crystallization in ceria films, as observed by XRD measurement.

It has been reported in literature that the higher is the Ce^{3+} content, the lower is the energy gap value [46]. The optical gap can be estimated by using ellipsometric data. In our case, and in perspective of CeO_2 integration in some devices, is relevant to understand if the Ce^{3+} amount and, more generally, the observed structural characteristics and chemical composition of CeO_2 films are sensible to a variation of the optical gap [47].

In **figure 5(a)** we report the raw ellipsometric data Ψ (open squares) and Δ (circles) of CeO_2/Si. The continuous lines superimposed to the data are the fitting curves obtained from two Tauc-Lorentz (2TL) dispersion model [48]. In **Table 3** the fit parameter values for both CeO_2/Si and

CeO_2/TiN are summarized. We used a simple three-layer model consisting of CeO_2/SiO_2-interfacial layer/Si film for CeO_2/Si, and a model consisting of CeO_2/TiN-oxidized/TiN/ SiO_2/Si for CeO_2/TiN. The model parameters for TiN layer were firstly determined by a preliminary measurement of such layer before their inclusion in the model for CeO_2/TiN.

Keeping CeO_2 layer thickness set as variable, the goodness of the chosen model is the correspondence of this thickness value with the thickness obtained by XRR. The obtained value of 24.5 nm (see **Table 3**) for CeO_2 on Si, in line with the XRR thickness (considering that the error in the XRR thickness equals to the surface roughness), corroborates the choice of two Tauc-Lorentz oscillators for optical data parametrization.

From the model, we extract the real (n) and imaginary (k) part of the refractive index in the range 1.24-5.05 eV, showed in **figure 5(b)** for CeO_2/Si. In particular, the n value is 2.3 at 2.25 eV (i.e. 550 nm of wavelength), which corresponds to the value estimated for plasma enhanced ALD-deposited CeO_2 film [16]. This value is in line with the refractive index found for CeO_2 deposited with other techniques [41], but lower than the value measured for highly oriented CeO_2 [49]. For CeO_2/TiN we obtain $n = 2.4$ at 2.25 eV, close to the value extracted for CeO_2 on Si.

From the extinction coefficient k, the plot $(\alpha h\nu)^2$ vs $h\nu$ e $(\alpha h\nu)^{1/2}$ vs $h\nu$ can be drawn, **figures 6(a)-(b)**. The optical band gap for the direct and indirect transitions are calculated as the intercept position of the extrapolated linear part of the curves. The obtained optical band gap for the direct transition is 3.54±0.63 eV and for the indirect transition is 2.89±0.19 eV for CeO_2/Si, **figure 6(a)**, and 3.63±0.18 eV and 3.05±0.22 eV for the direct and indirect transition for CeO_2/TiN, **figure 6(b)**. These values are in good agreement with literature [16, 46, 47]. Our findings suggest that the optical properties of CeO_2 are not affected by the differences arisen from the detailed structural and chemical analysis of the films.

Conclusions

In summary, in this work we report about a detailed structural and chemical characterization of CeO_2 thin films deposited by ALD on both Si and TiN substrates. The ALD growth of the cerium oxide resulted in a polycrystalline structure as expected from previous reports, however with a preferred orientation of the grains depending on the substrate. In particular, we observe an enhancement of the diffraction signal connected to the <100> orientation of the grains in the case of Si substrate, compared to the enhancement of the diffraction signal related to the <111> direction for the TiN substrate. The not-favoured exposure of *(100)* planes for strongly ionic oxide like CeO_2 can be explained considering the higher interface CeO_2/TiN roughness compared to CeO_2/Si one, which can contribute in a change to the energy requirement for the nucleation of crystals with *(111)* orientation. Additionally, the presence of defects or charge compensating species, i.e. oxygen vacancy due to Ce^{3+}: Ce^{4+} substitution, can contribute to the balance of the energy requirement. As a perspective for future work, it could be of interest to determine the stoichiometry of the CeO_2 in the first layers in contact with the substrate, in order to clarify the role of the interface in dictating the structural properties of the oxide.

However, our study evidences that the substrate plays a role in the growth of CeO_2 films by ALD, contributing to boost the consideration for ALD based processes targeting a wide range of applications and a viable route for ceria oxide engineering to address optimal properties for specific applications, such as in microelectronics and catalysis.

AUTHOR INFORMATION

Corresponding Author

*S. Vangelista, silvia.vangelista@mdm.imm.cnr.it

Author Contributions

The manuscript was written through contributions of all authors. All authors have given approval to the final version of the manuscript.

Funding Sources

This work was partially supported by ECSEL-JU R2POWER300 project under grant agreement n.653933.

ACKNOWLEDGMENTS

The authors would thank Dr. Sabina Spiga for fruitful discussions, Dr. Elena Cianci (IMM-CNR) for discussions on SE measurements and modelling, Daniela Brazzelli, Fabrizio Toia and Donata Piccolo (ST Agrate) for discussions on sample preparation and Davide Codegoni (ST Physics Lab Agrate) for TEM data and discussion.

FIGURES CAPTIONS

Figure 1. XRR experimental curves and data fitting of the as-deposited CeO_2 on Si **(a)** and on TiN **(b)** substrates; the corresponding AFM image of the sample is shown as inset.

Figure 2. GIXRD experimental pattern and data fitting of as-deposited CeO_2 on Si (light blue circles and continuous blue line) and on TiN (black squares and continuous red line) substrates. The pink line is the diffraction powder pattern from cubic (*Fm-3m*) CeO_2 used as reference [35].

Figure 3. ToF-SIMS depth profile of CeO_2 and corresponding EDX maps; **(a)** on Si and **(b)** on TiN substrate.

Figure 4. **(a)** *Ce 3d* XPS spectra (both experimental and fitting curves) collected at take-off angle of 45° from CeO_2 on Si (upper panel) and on TiN (lower panel). The fit components of the Ce^{3+} and Ce^{4+} – related doublets are also shown; **(b)** *O 1s* XPS spectra (experimental and fitting curves) from CeO_2 on Si (upper panel) and on TiN (lower panel). The 2 components of the profile deconvolution are also shown.

Figure 5. **(a)** Spectroscopic ellipsometric data (open circles and squares) obtained from CeO_2 on Si. The full lines are the fit from the dispersion model (2TL); **(b)** real (*n*) and imaginary (*k*) part of the refractive index obtained from the model.

Figure 6. Plot of $(\alpha h\nu)^2$ as a function of photon energy (blue open squares); from the linear part of the plot (light blue continuous line) we obtain the direct optical band gap. Plot of $(\alpha h\nu)^{1/2}$ as a function of photon energy (black open triangles); from the linear part of the plot (red continuous line) the indirect optical band gap is obtained. (a) CeO_2/Si; (b) CeO_2/TiN.

REFERENCES

[1] C.T. Campbell, C.H.F. Peden, Oxygen Vacancies and Catalysis on Ceria Surfaces, Science 309(5735) (2005) 713.

[2] J. Kugai, S. Velu, C. Song, Low-temperature reforming of ethanol over CeO_2-supported Ni-Rh bimetallic catalysts for hydrogen production, Catalysis Lett. 101(3-4) (2005) 255.

[3] A. Trinchi, Y.X. Li, W. Wlodarski, S. Kaciulis, L. Pandolfi, S. Viticoli, E. Comini, G. Sberveglieri, Investigation of sol–gel prepared CeO_2–TiO_2 thin films for oxygen gas sensing, Sens. Actuators B 95(1−3) (2003) 145.

[4] D. Barreca, E. Comini, A. Gasparotto, C. Maccato, C. Maragno, G. Sberveglieri, E. Tondello, Gas Sensing Properties of Columnar CeO_2 Nanostructures Prepared by Chemical Vapor Deposition. J. Nanosci. Nanotech. 8(2) (2008) 1012.

[5] H. Yokokawa, T. Horita, High-temperature solid oxide fuel cells: fundamentals, design and applications, (2003) chapt. 5, pages 119–147, S.C. Singhal and K. Kendall, eds.; Elsevier.

[6] F.-C. Chiu, C.-M. Lai, Optical and electrical characterizations of cerium oxide thin films. J. Phys. D: Appl. Phys. 43 (2010) 075104.

[7] L. Tye, N.A. El-Masry, T. Chikyow, P. McLarty, S.M. Bedair, Electrical characteristics of epitaxial CeO_2 on Si(111), Applied Physics Letters 65 (1994) 3081.

[8] L. Tye, N.A. El-Masry, T. Chikyow, P. McLarty, S.M. Bedair, Electrical characteristics of epitaxial CeO_2 on Si(111), Applied Physics Letters 65 (1994) 3081.

[9] C. Dou, K. Kakushima, P. Ahmet, K. Tsutsui, A. Nishiyama, N. Sugii, K. Natori, T. Hattori, H. Iwai, Resistive switching behavior of a CeO_2 based ReRAM cell incorporated with Si buffer layer. Microelectronics Reliability, Advances in non-volatile memory technology 52 (2012) 688.

[10] P. Luches, and S. Valeri, Structure, Morphology and Reducibility of Epitaxial Cerium Oxide Ultrathin Films and Nanostructures, Materials 8(9) (2015) 5818.

[11] J.C. Wang, K.C. Chang, T.F. Lei, C.L. Lee, Carrier Transportation of Rapid Thermal Annealed CeO_2 Gate Dielectrics, Electrochem. Solid State Lett. 7 (2004) E55.

[12] Y. Zhu, N. Jain, M.K. Hudait, D. Maurya, R. Varghese, S. Priya, X-ray photoelectron spectroscopy analysis and band offset determination of CeO_2 deposited on epitaxial (100), (110), and (111) Ge, J. Vac. Sci. Technol. B 32 (2014) 011217.

[13] L. Kim, J. Kim, D. Jung, C.-Y. Park, C.-W. Yang, and Y. Roh, Effects of deposition parameters on the crystallinity of CeO_2 thin films deposited on Si(100) substrates by r.f.-magnetron sputtering, Thin Solid Films 360(1–2) (2000) 154.

[14] M. Kouda, K. Ozawa, K. Kakushima, P. Ahmet, H. Iwai, Y. Urabe, T. Yasuda, Preparation and Electrical Characterization of CeO_2 Films for Gate Dielectrics Application: Comparative Study of Chemical Vapor Deposition and Atomic Layer Deposition Processes, Japn. J. Appl. Phys. 50 (2011) 10PA06.

[15] D. Barreca, A. Gasparotto, E. Tondello, C. Sada, S. Polizzi, and A. Benedetti, Nucleation and Growth of Nanophasic CeO_2 Thin Films by Plasma-Enhanced CVD. Chem. Vap. Deposition 9 (2003) 199.

[16] D. Barreca, A. Gasparotto, C. Maccato, C. Maragno, and E. Tondello, Toward the Innovative Synthesis of Columnar CeO_2 Nanostructures. Langmuir 22(21) (2006) 8639.

[17] D. Barreca, G. Bruno, A. Gasparotto, M. Losurdo, E. Tondello, Nanostructure and optical properties of CeO_2 thin films obtained by plasma-enhanced chemical vapor deposition. Mater.Sci. Engin.: C, 23(6-8) (2003) 1013.

[18] L. Armelao, D. Barreca, G. Bottaro, A. Gasparotto, E. Tondello, Plasma-Enhanced CVD CeO_2 Nanocrystalline Thin Films Analyzed by XPS. Surf. Sci. Spectra 8 (2001) 247.

[19] Y.-M. Chiang, E.B. Lavik, I. Kosacki, H.L. Tuller, and J.Y. Ying, Defect and transport properties of nanocrystalline CeO_{2-x}, Appl. Phys. Lett. 69 (1996) 185.

[20] M. Coll, J. Gazquez, A. Palau, M. Varela, X. Obradors, and T. Puig, Low Temperature Epitaxial Oxide Ultrathin Films and Nanostructures by Atomic Layer Deposition, Chem. Mat. 24(19) (2012) 3732.

[21] W.-H. Kim, W.J. Maeng, M.-K. Kim, J. Gatineau, H. Kim, Electronic Structure of Cerium Oxide Gate Dielectric Grown by Plasma-Enhanced Atomic Layer Deposition, J. Electrochem. Soc. 158 (2011) G217.

[22] J. Päiväsaari, M. Putkonen, L. Niinistö, Cerium dioxide buffer layers at low temperature by atomic layer deposition, J. Mater. Chem. 12 (2002) 1828.

[23] J.S. Wrench, K. Black, H.C. Aspinall, A.C. Jones, J. Basca, P.R. Chalker, P.J. King, M. Werner, H.O. Davies, P.N. Heys, MOCVD and ALD of CeO_2 Thin Films using a Novel Monomeric Ce^{IV} Alkoxide Precursor, Chem. Vap. Dep. 15 (2009) 259.

[24] P.J. King, M. Werner, P.R. Chalker, A.C. Jones, H.C. Aspinall, J. Basca, J.S. Wrench, K. Black, H.O. Davies, P.N. Heys, Effect of deposition temperature on the properties of CeO_2 films grown by atomic layer deposition, Thin Solid Films 519 (2011) 4192.

[25] W.-H Kim, M.-K. Kim, W.J. Maeng, J. Gatineau, V. Pallem, C. Dussarat, A. Noori, D. Thompson, S. Chu and H. Kim, Growth Characteristics and Film Properties of Cerium Dioxide Prepared by Plasma-Enhanced Atomic Layer Deposition, J. Electrochem. Soc. 158 (2011) G169.

[26] T.V. Ivanova, J. Toivonen, P. S. Maydannik, T. Kääriäinen, M. Sillanpää, T. Homola and D. C. Cameron, Atomic layer deposition of cerium oxide for potential use in diesel soot combustion, J. Vac. Sci.& Techn. A 34(3) (2016) 031506.

[27] Z.Fan, J. An, A. Iancu, F. B. Prinz, Thickness effects of yttria-doped ceria interlayers on solid oxide fuel cells, J. Power Sourc.218 (2012) 187.

[28] L. Lutterotti, S. Matthies, H.-R. Wenk, MAUD: a friendly Java program for material, IUCr Newsletter of CPD 21 (1999) 14.

[29] C. Wiemer, S. Ferrari, M. Fanciulli, G. Pavia, L. Lutterotti, Combining grazing incidence X-ray diffraction and X-ray reflectivity for the evaluation of the structural evolution of HfO_2 thin films with annealing. Thin Solid Films 450(1) (2004) 134.

[30] A. Lamperti, E. Cianci, O. Salicio, L. Lamagna, S. Spiga, M. Fanciulli, Thermal stability of high-κ oxides on SiO_2/Si or Si_xN_y/SiO_2/Si for charge-trapping nonvolatile memories, Surface and Interface Analysis, 45(1) (2013) 390.

[31] D. Sangalli, A. Lamperti, E. Cianci, R. Ciprian, M. Perego, and A. Debernardi, Role of oxygen vacancies on the structure and density of states of iron-doped zirconia, Phys. Rev. B, 87(8) (2013) 085206.

[32] S. Vangelista, E. Cinquanta, C. Martella, M. Alia, M. Longo, M. Lamperti, R. Mantovan, F. Basso Basset, F. Pezzoli, and A. Molle, Towards a uniform and large-scale deposition of MoS_2 nanosheets via sulfurization of ultra-thin Mo-based solid films, Nanotech. 27(17) (2016) 175703.

[33] D. Briggs, M.P. Seah, Practical Surface Analysis by Auger and X-ray Photoelectron Spectroscopy, Wiley, New York, (1984).

[34] X.Q. Fu, C. Wang, H.C. Yu, Y.G. Wang, T.H. Wang, Fast humidity sensors based on CeO_2 nanowires, Nanotechn. 18 (2007) 145503.

[35] ICSD no. 621705, from NIST/FIZ FindIt searches Inorganic Crystal Structure Database.

[36] D. Barreca, A. Gasparotto, C. Maccato, C. Maragno, E. Tondello, E. Comini, and G. Sberveglieri, Columnar CeO_2 nanostructures for sensor application, Nanotechn. 18(12) (2007) 125502.

[37] T.X.T. Sayle, S.C. Parker, C.R.A. Catlow, The role of oxygen vacancies on ceria surfaces in the oxidation of carbon monoxide, Surf. Sci. 316 (1994) 329.

[38] D.C. Sayle, S.A. Maicaneanu, G.W. Watson, Atomistic Models for CeO_2(111), (110), and (100) Nanoparticles, Supported on Yttrium-Stabilized Zirconia, J. Am. Chem. Soc. 124 (2002) 11429.

[39] S. Zhu, D.H. Lowndes, J.D. Budai, D.P. Norton, In-plane aligned CeO_2 films grown on amorphous SiO_2 substrates by ion-beam assisted pulsed laser deposition, Appl. Phys. Lett. 65 (1994) 2012.

[40] A. Trovarelli, Catalysis by Ceria and Related Materials, World Scientific (2002)

[41] E. Mamontov, T. Egami, R. Brezny, M. Koranne, S. Tyagi, Lattice Defects and Oxygen Storage Capacity of Nanocrystalline Ceria and Ceria-Zirconia, J. Phys. Chem. B 104 (2000) 11110.

[42] F. Pagliuca, P. Luches, S. Valeri, Interfacial interaction between cerium oxide and silicon surfaces. Surf. Sci. 607 (2013) 164.

[43] C. Anandan, P. Bera, XPS studies on the interaction of CeO_2 with silicon in magnetron sputtered CeO_2 thin films on Si and Si_3N_4 substrates, Appl. Surf. Sci. 283 (2013) 297.

[44] Y. Zhu, N. Jain, M.K. Hudait, D. Maurya, R. Varghese, Priya, S. X-ray photoelectron spectroscopy analysis and band offset determination of CeO_2 deposited on epitaxial (100), (110), and (111)Ge, J. Vac. Sci. Tech. B 32 (2014) 11217.

[45] D.L. Perry, L.Tsao, H.G. Brittain, X-ray photoelectron and infrared spectroscopic studies of the decarboxylation/oxidation of cerium(Ill) carbonate octahydrate, J. Mater. Sci. Lett. 3 (1984) 1017.

[46] P. Patsalas, S. Logothetidis, C. Metaxa, Optical performance of nanocrystalline transparent ceria films Appl. Phys. Lett. 81 (2002) 466.

[47] L. Méchin, A. Chabli, F. Bertin, M. Burdin, G. Rolland, C. Vannuffel, J.-C. Villégier, A combined x-ray specular reflectivity and spectroscopic ellipsometry study of CeO_2/yttria-stabilized-zirconia bilayers on Si(100) substrates, J. Appl. Phys. 84 (1998) 4935.

[48] M. Losurdo, Relationships among surface processing at the nanometer scale, nanostructure and optical properties of thin oxide films, Thin Solid Films 455–456 (2004) 301.

[49] S. Guo, H. Arwin, S.N. Jacobsen, K. Järrendahl, U. Helmersson, A spectroscopic ellipsometry study of cerium dioxide thin films grown on sapphire by rf magnetron sputtering J. Appl. Phys. 77 (1995) 5369.

TABLES

Table 1. Properties of CeO_2 grown on Si and on TiN from XRR and XRD data fitting.

Sample ID	Thickness (nm)	Interface roughness (nm)	Surface roughness (nm)	El. Density (e/Å^3)	Grain size (nm)	
					(111)	*(200)*
CeO_2 on Si	23.8±0.3	0.3±0.1	1.3±0.1	1.69±0.05	8.0±0.1	11.6±0.1
CeO_2 on TiN	23.8±0.2	0.8±0.1	1.4±0.1	1.65±0.05	8.3±0.1	11.4±0.1

Table 2. XPS peak assignment, positions and relative area of Ce_{3d} peaks. The areas of the different components are used to calculate the percentage of Ce^{3+} and Ce^{4+}.

Sample ID	Peak assignment	Ce species	Binding energy (eV)	Relative area (%)
CeO_2 on Si	v_0	Ce^{3+}	882.0	9
	v	Ce^{4+}	882.4	24
	v’	Ce^{3+}	885.3	6
	v’’	Ce^{4+}	888.5	10
	v’’’	Ce^{4+}	898.1	18
	u_0	Ce^{3+}	900.3	4
	u	Ce^{4+}	900.7	12
	u’	Ce^{3+}	903.6	3
	u’’	Ce^{4+}	906.8	5
	u’’’	Ce^{4+}	916.3	9
Percentage of Ce_2O_3 = 22 %				
Percentage of CeO_2 = 78 %				
CeO_2 on TiN	v_0	Ce^{3+}	881.9	7
	v	Ce^{4+}	882.4	21
	v’	Ce^{3+}	885.1	5
	v’’	Ce^{4+}	888.5	12
	v’’’	Ce^{4+}	897.9	21
	u_0	Ce^{3+}	900.2	3
	u	Ce^{4+}	900.7	11
	u’	Ce^{3+}	903.4	3
	u’’	Ce^{4+}	906.8	6
	u’’’	Ce^{4+}	916.3	11
Percentage of Ce_2O_3 = 18 %				
Percentage of CeO_2 = 82 %				

Table 3. 2TL model parameters for the CeO_2 film on Si and TiN. ε_∞ is the value of real part of the dielectric function ε at infinite energy, Eg is the bandgap of the material, A is the oscillator amplitude, E0 is the energy (position) of the Lorentz peak, and C is the broadening parameter.

Sample ID	Thickness CeO_2 (nm)	ε_∞ (eV)	A1	Eg1 (eV)	E01 (eV)	C1	A2	Eg2 (eV)	E02 (eV)	C1
CeO_2 on Si	24.5±0.01	2.4±0.1	51.6±1.1	2.8±0.01	3.9±0.01	0.8±0.01	41.8±4.5	2.9±0.01	6.4±0.1	4.5±0.7
CeO_2 on TiN	25.0±0.01	1.7±0.1	87.1±2.0	3.0±0.01	3.8±0.01	0.8±0.01	31.1±3.5	3.1±0.01	7.0±0.1	2.9±0.5

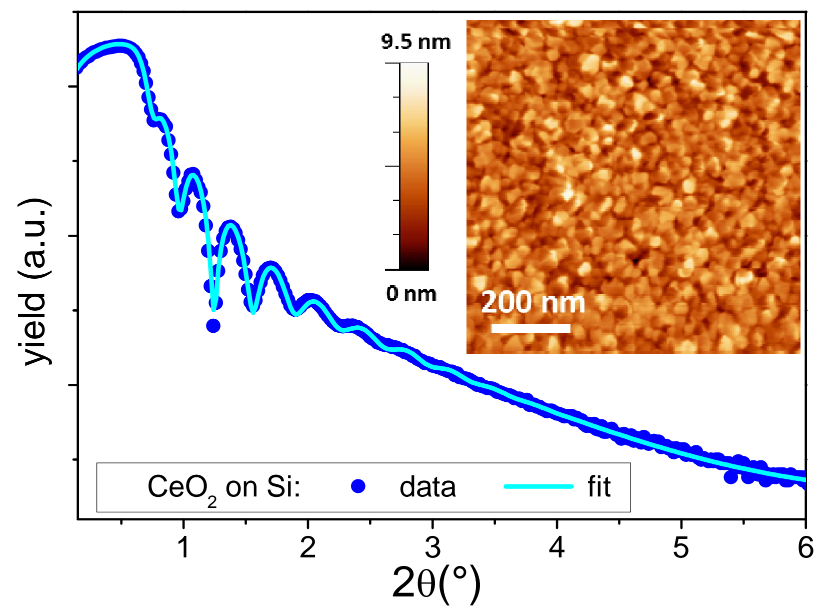

(a)

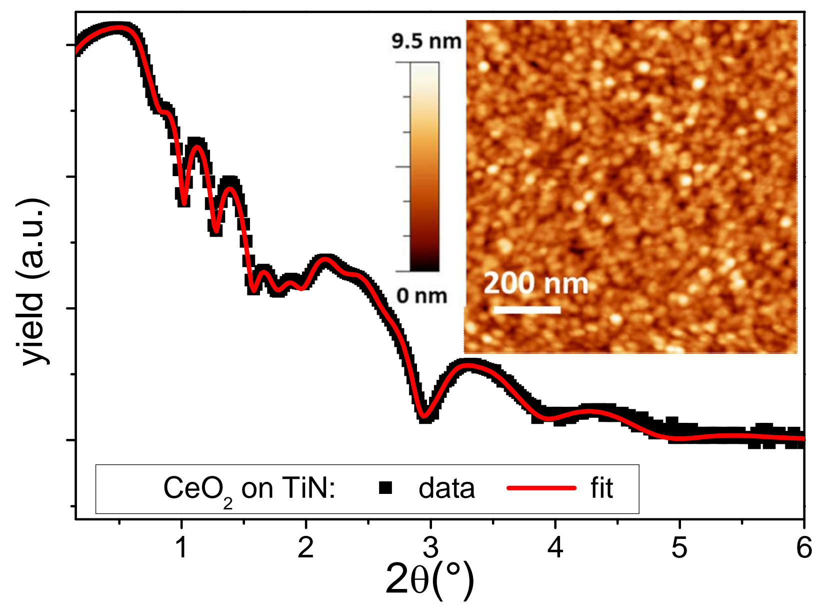

(b)

Figure 1

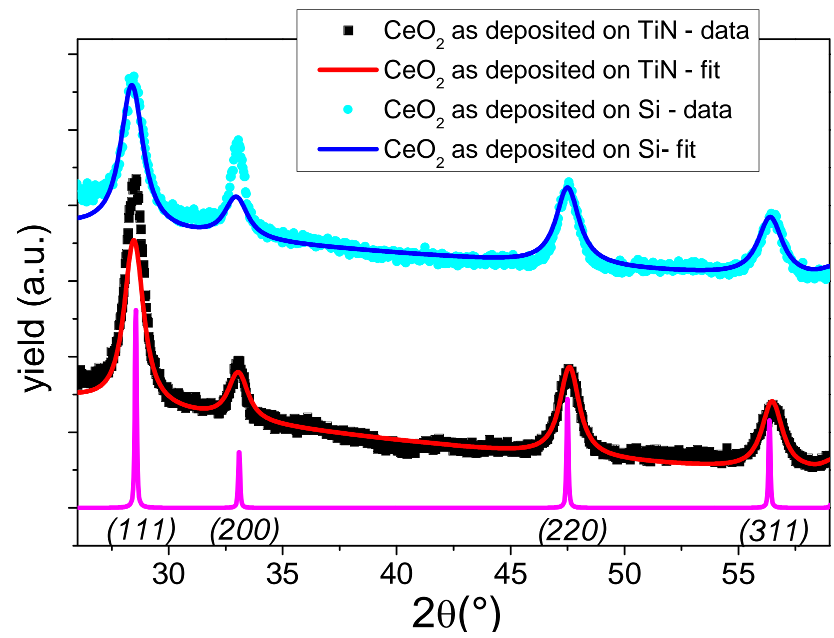

Figure 2

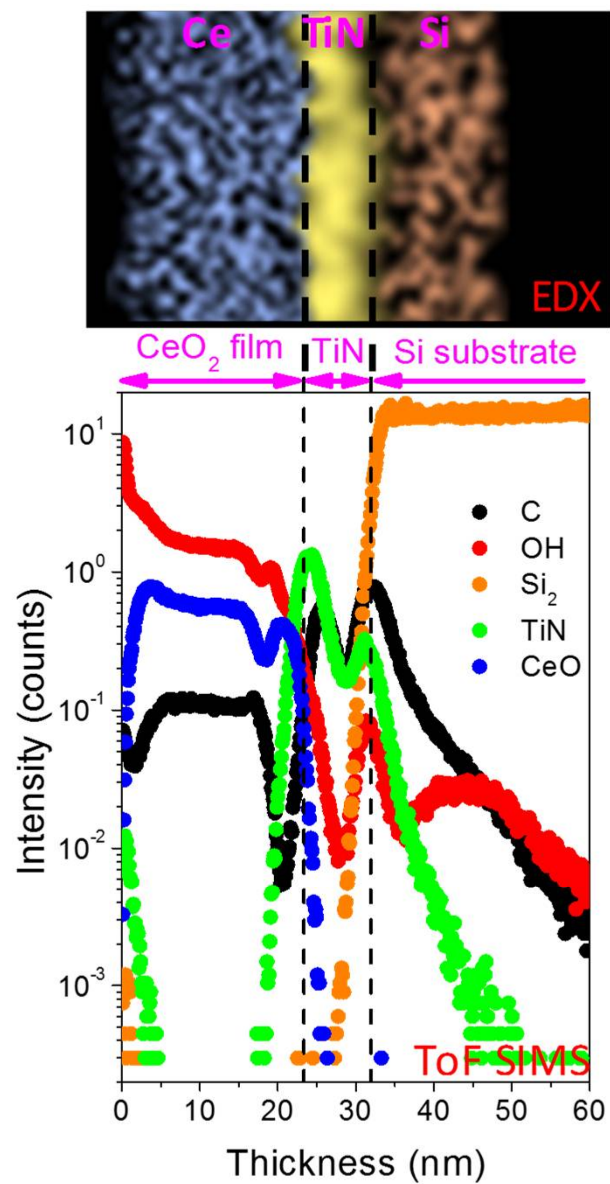

(a)

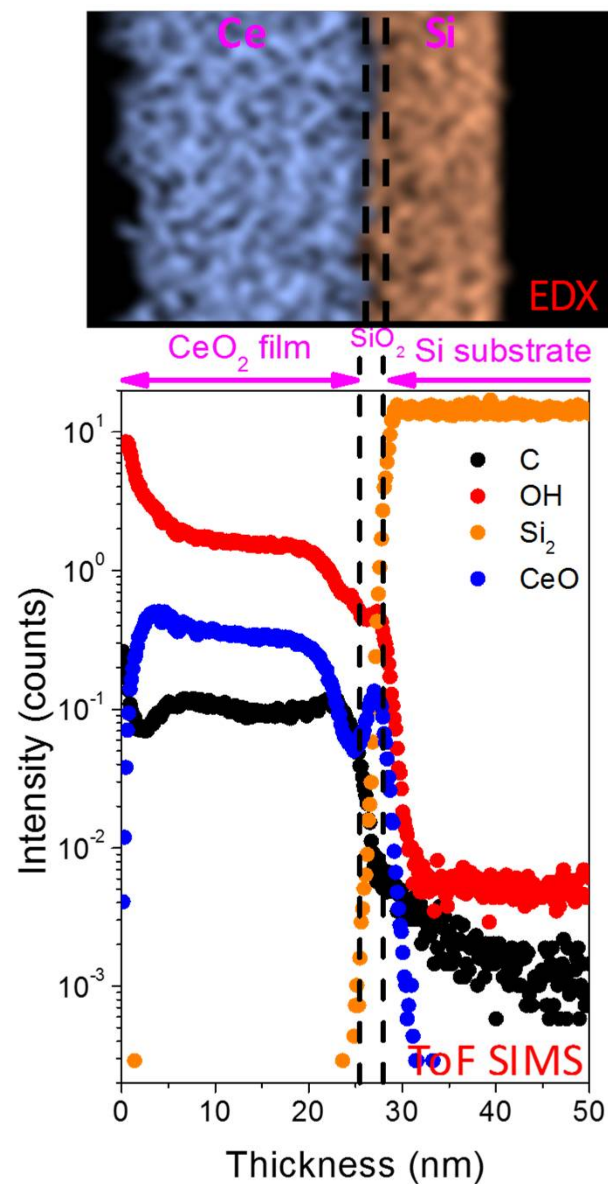

(b)

Figure 3

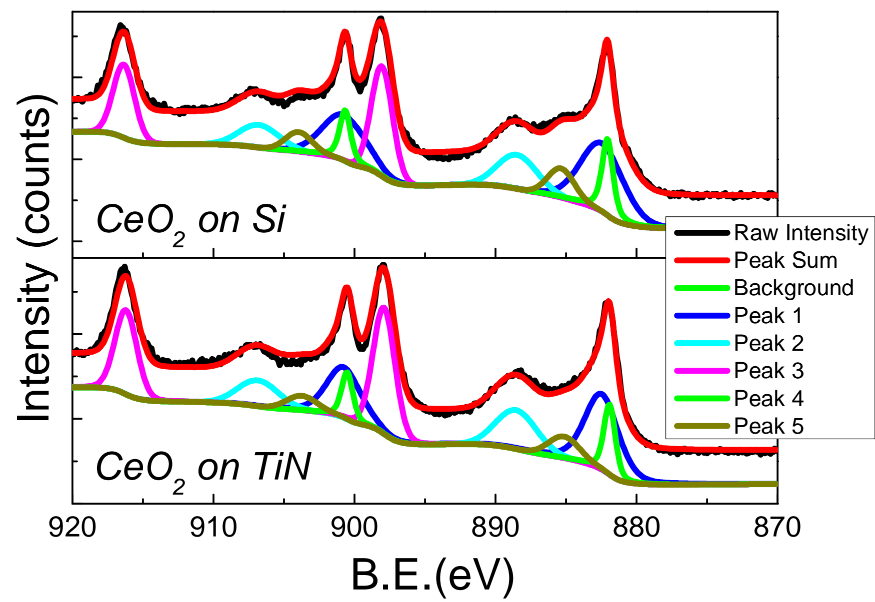

(a)

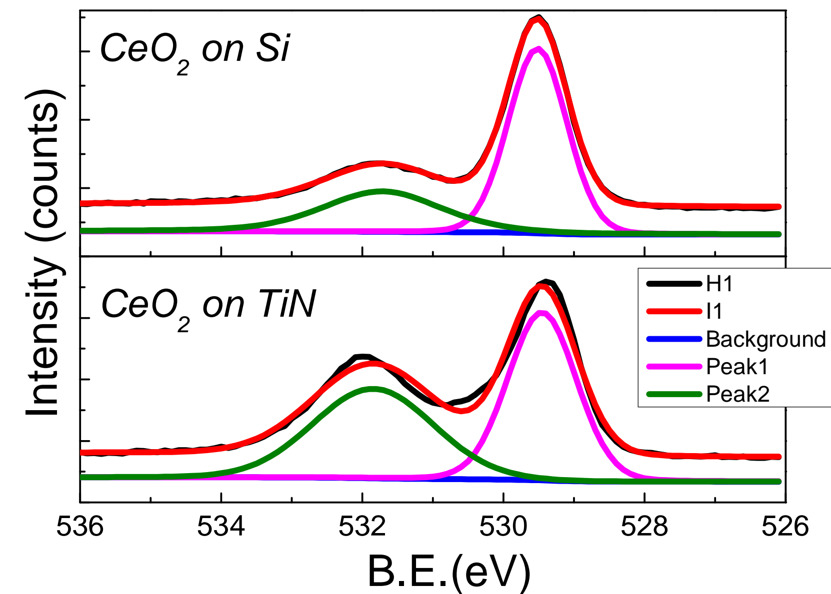

(b)

Figure 4

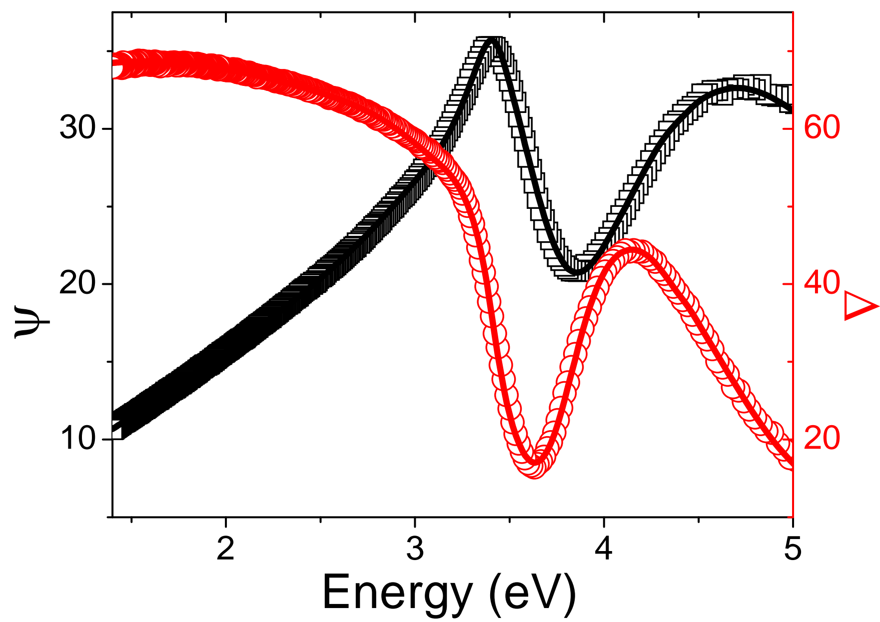

(a)

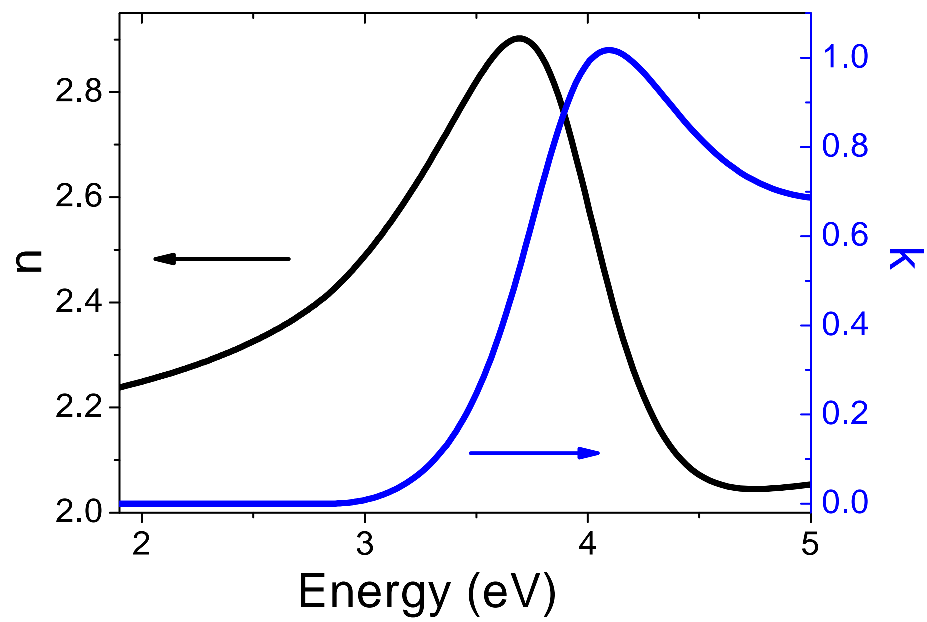

(b)

Figure 5

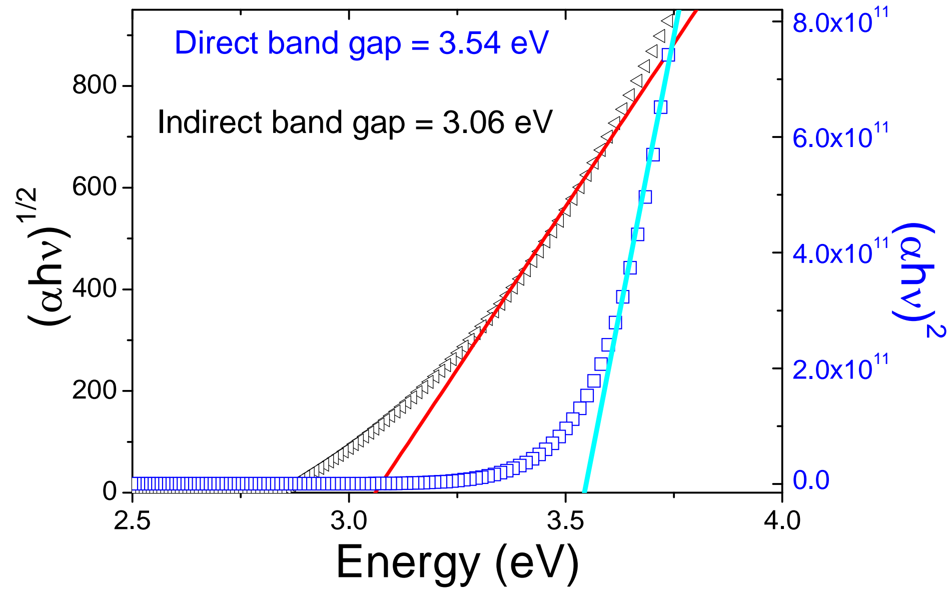

(a)

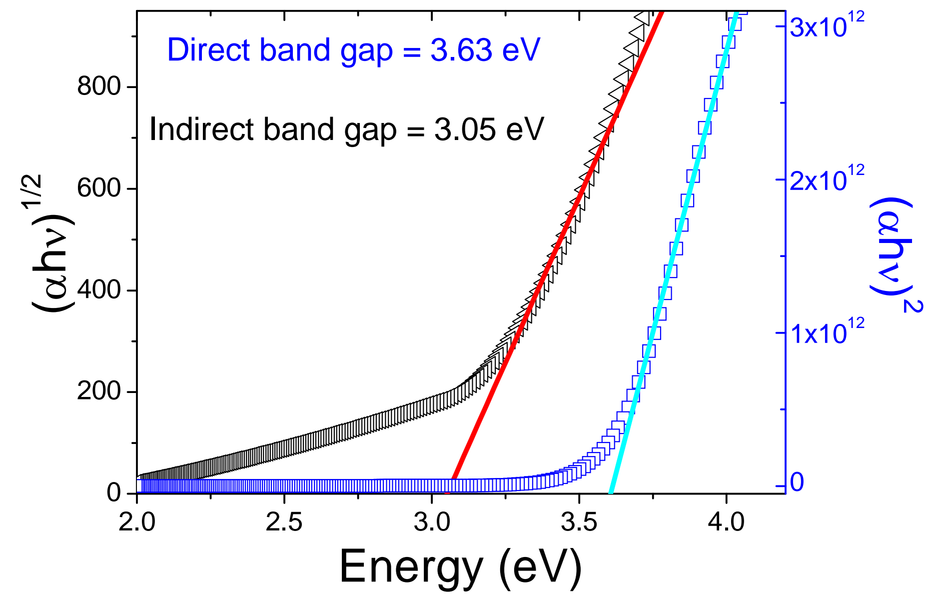

(b)

Figure 6